Climent, A.; Guillem Sánchez, MS.; Fuentes, L.; Lee, P.; Bollensdorff, C.; Fernandez-Santos, M.; Suarez-Sancho, S.... (2015). Role of atrial tissue remodeling on rotor dynamics an in vitro study. AJP - Heart and Circulatory Physiology. 309(11):H1964-H1973. doi:10.1152/ajpheart.00055.2015.

Title:

The Role of Atrial Tissue Remodeling on Rotor Dynamics: An In-Vitro Study

Authors:

Andreu M Climent[1], María S Guillem[2], Lucia Fuentes[1], Peter Lee[3,4], Christian Bollensdorff[5], María Eugenia Fernández-Santos[1], Ricardo Sanz-Ruiz[1], Pedro Luis Sánchez[1], Felipe Atienza[1], Francisco Fernández-Avilés[1]

Affiliation:

[1] Cardiology Department, Hospital General Universitario Gregorio Marañón, Instituto de Investigación Sanitaria Gregorio Marañón, Madrid, Spain

[2] ITACA Institute, Universitat Politécnica de Valencia, Valencia, Spain

[3] Essel Research and Development Inc., Toronto, Canada

[4] Division of Cardiology, Toronto General Hospital, Toronto, Canada

[5] Qatar Cardiovascular Research Center, Qatar Foundation, Doha, Qatar

Running Head:

In-Vitro Atrial Tissue Remodeling

Address for correspondence:

Andreu M. Climent (acliment@cardiovascularcelltherapy.com). Laboratory of Bioartificial Organs. Department of Cardiology. Instituto de Investigación Sanitaria Gregorio Marañón. Hospital GU Gregorio Marañón. Edificio Materno Infantil. c\ O'Donnell 48, 28009, Madrid, España +34915290520

Authors contributions:

AMC, MSG, FA and FFA. Conception and design of research; AMC, LF, PL, CB, MEFS performed experiments; AMC, MSG, LF analyzed data; AMC, MSG, PL, CB, RSR, PLS, FA, FAF interpreted results of experiments; AMC and MSG prepared figures and drafted the manuscript; AMC, MSG, LF, PL, CB, MEFS, RSR, PLS, FA and FFA edited and revised manuscript and approved final version of manuscript.

ABSTRACT

The objective of this article is to clarify the mechanisms underlying the increase in electrophysiological complexity related to atrial fibrillation (AF) caused by electrophysiological and structural tissue remodeling. We analyze the modifications of rotor dynamics following tissue remodeling in an in-vitro model of AF.

Atrial murine cells (HL-1 myocytes) were maintained in culture after the spontaneous initiation of AF and analyzed at two later time points: 3.1±1.3 and 9.7±0.5 days after AF initiation. The electrophysiological characteristics of in-vitro fibrillation (e.g. phase singularities per square centimeter, PS/cm^2, dominant frequency and rotor meandering) analyzed by means of optical mapping were compared with the degree of electrophysiological remodeling (i.e. relative gene expression of key ion channels) and structural inhomogeneity.

The number of singularity points per square centimeter at baseline was significantly higher in late compared to early stage cultures (i.e. 1.12±0.14 vs. 0.43±0.19 PS/cm^2, $p<0.01$). This increase in electrophysiological complexity was correlated with ion channel gene expression modifications associated with atrial tissue remodeling (i.e. CACN1C, SCN5A and KCND3 decreased; KCNJ2 increased) and showed a direct correlation with the degree of structural inhomogeneity in microscopy images ($R2=0.78$, $p<0.01$). Changes in fibrillation complexity from early to late stages were associated with changes in reentrant patterns (i.e. decrease in rotor tip meandering and increase in wavefront curvature).

Modifications in rotor dynamics may underlie the increased complexity of remodeled cell cultures and arise as potential targets for arrhythmia termination.

KEYWORDS

Atrial Fibrillation; Tissue Remodeling; Optical Mapping; Rotor Dynamics

I. INTRODUCTION

Atrial fibrillation (AF) requires a triggering mechanism and a cardiac substrate that allows the perpetuation of the reentrant activity (13). Studies have shown that in paroxysmal AF, the arrhythmia is hierarchically maintained by a limited number of regions preferentially located at the pulmonary veins (PV) that can be eliminated by means of targeted radiofrequency ablation (3, 4, 11). However, in chronic AF patients more extensive ablation strategies are needed to restore sinus rhythm. It is believed that this is a consequence of tissue remodeling in the atrium (7). Specifically, remodeling refers to changes in atrial tissue structural and electrophysiologic properties following periods of sustained AF (30).

The evaluation of antiarrhythmic treatments which can mitigate or reverse the effects of remodeling and restore sinus rhythm in chronic AF requires the development of experimental models that reproduce key features of electrical and/or structural remodeling. However, the development of effective research models of chronic AF is one of the main barriers to elucidating the underlying mechanisms of this arrhythmia and enabling design of effective therapies. Atrial murine immortalized cells (HL-1) under conditions of fast activation rates display some characteristics consistent with fibrillation-related remodeling as those found in atrial tissue from patients with chronic AF (6, 27, 28). Building on these results, we have analyzed the relation between HL-1 cell culture remodeling and the electrophysiological complexity of fibrillation patterns. Despite the limitations of any in-vitro cell culture model, the present model of the transition from paroxysmal to chronic AF reproduces to some extent the different degrees of electrophysiological complexity observed in patients with AF associated with varying degrees of electrophysiological and structural remodeling (2).

In the present study, we analyzed the mechanisms of rotor dynamics that promote increased fibrillation complexity and related them to electrophysiological remodeling and structural inhomogeneities arising from sustained in vitro arrhythmia. Finally, we tested the hypothesis that a reduction the in rotor core excitability would increase their meandering and promote the termination of the arrhythmia by collisions, either between rotors or with anatomical obstacles.

II. METHODS

Experimental protocol. HL-1 cells were maintained, grown and proliferated according to the protocol established by Claycomb et al. (8). Under these culture conditions, cells spontaneously presented fibrillatory activity after a mean of 53±17 hours, as detected by measuring the activation rate in bright-field microscopy videos. During spontaneous non-fibrillatory activation, HL-1 cells showed a slow activation rate of 1.4±0.5 beats per second. After achieving further cell confluency, the HL-1 cell monolayers sustained faster fibrillatory rates of 3.1±0.2 Hz. In order to evaluate time dependent effects of fibrillation on AF complexity, cell cultures were divided into two groups based on incubation period passed after the initiation of AF: (A) Early: 3.1±1.3 days (N=10) and (B) Late: 9.7±0.5 days (N=8). For each group, optical mapping recordings (4 seconds in duration) were acquired under basal conditions and after the administration of verapamil (4 μM in Krebs solution). In addition to calcium imaging, (1) structural homogeneity was assessed by analyzing bright-field microscopy images from several regions across the dish and (2) electrophysiological remodeling was evaluated by reverse transcription polymerase chain reaction (RT-PCR) process.

Calcium Dye Loading: For calcium transient (CaT) imaging, HL-1 cell cultures were stained by immersion in Claycomb culture medium with rhod-2 AM (Ca^{2+} sensitive probe, TEFLabs, Inc, Austin, TX. USA) dissolved in DMSO (1 mM stock solution; 3.3 μl per ml in culture medium) and Probenecid (TEFLabs, Inc, Austin, TX, USA) at 420 μM for 30 minutes under incubation conditions. After dye incubation, culture medium was changed to fresh modified Krebs solution at 36.5ºC (containing, in mM: NaCl, 120; $NaHCO_3$ 25; $CaCl_2$ 1.8; KCl 5.4; $MgCl_2$ 1; glucose 5.5; $H_2O_4PNa{\bullet}H_2O$ 1.2). All chemicals were obtained from Sigma-Aldrich (Dorset, UK) or Fisher Scientific Inc. (New Jersey, USA).

Optical mapping: In order to excite rhod-2, cell cultures were illuminated with a filtered green LED light source: LED: CBT-90-G (peak power output 58 W; peak wavelength 524 nm; Luminus Devices, Billerica, USA), with a plano-convex lens (LA1951; focal length= 25.4 mm; Thorlabs, New Jersey, USA) and a green excitation filter (D540/25X; Chroma Technology, Bellows Falls, USA). Two such light sources were used to achieve homogeneous illumination. Fluorescence was recorded with an electron-multiplying charge-coupled device (EMCCD; Evolve-128: 128x128, 24x24 μm-square pixels, 16 bit; Photometrics, Tucson, AZ, USA), with a custom emission filter (ET585/50-800/200M; Chroma

Technology) suitable for rhod-2 emission placed in front of a high-speed camera lens (DO-2595; Navitar Inc., Rochester, USA).

Calcium Image processing. Custom software written in MATLAB was used to perform optical mapping image processing. Specifically, the organization of fibrillatory activity was estimated as the mean number of simultaneous functional reentrant activities. Those reentries were automatically identified as singularity points that remained stable over time and space by applying phase map analysis. Phase maps of each movie were obtained by calculating the instantaneous phase of the Hilbert-transformed optical recordings (31). The phase signal ranges between 0 and 2π represent the relative delay of each signal in one period. A singularity point was defined as the point in a phase map which is surrounded by phases from 0 to 2π. These phase transitions were evaluated at 3 concentric circles centered at each evaluated point. Phase singularities (PS) were defined as points at which the phase in at least two of these three circles were required to fulfill two conditions: (a) phase transition between two consecutive pixels not exceeding 0.6 π; and (b) monotonic phase changes. Once all singularity points were identified, they were connected in time and space into rotors. Unstable rotors with durations of less than 100ms were discarded. The complexity of the fibrillatory activity was defined as the mean number of simultaneous functional reentries per square centimeter. Finally, the trajectory of PS was tracked and the mean distance traveled by each rotor was calculated.

In order to estimate rotor curvature, lines connecting phase transitions from 0 to 2π that originate at each rotor were selected. These transition lines were traced from the rotor tip to the periphery and the relative angle (α) and distance (δ) of line points with respect to the rotor tip was computed. The curvature at each point in the transitional line was measured as the spatial derivative of α ($d\alpha/d\delta$). Finally, the curvature of the rotor was estimated as the mean value of curvature along the transitional line.

Power spectra of optical signals were estimated by using Welch periodogram (2-second Hamming window overlap). Dominant frequency (DF) of each pixel was determined as the frequency with the largest peak in the spectrum between 0.05 and 30 Hz. For each individual cell culture, the highest DF was defined as the maximum DF of the entire dish.

Gene expression analysis. Total RNA from HL1 cell cultures of both groups were isolated using Tri-reagent (Sigma). Transcripts were quantified in a two-step RT-PCR. First-strand cDNA was synthesized using the High Capacity cDNA Reverse Transcription Kit (Applied Biosystems) with random hexamers.

Then, samples were run using SYBR Green oligonucleotides and the CFX Real Time PCR detection Systems (Bio Rad). The analysis was customized, with three biological replicates per target gene, and two technical replicates for each sample. Gene expression values were normalized to two standard housekeeping genes (36b4 and Cyclophylin) as internal controls, and expressed as relative mRNA levels (relative expression). Data were automatically analyzed using the CFX gene expression analysis software (Bio Rad). Primer sequences are summarized in table 1.

Immunohistochemistry and microscopy. In order to quantify the degree of structural heterogeneities produced during the long incubation times, the inhomogeneity of cell cultures was quantified based on the gray level co-occurrence matrix of bright field images (12). This indirect measurement was validated by means the correlation of the mentioned inhomogeneity with the number of cell nuclei measured in a subset of cell cultures labeled with 4′,6-diamidino-2-phenylindole, DAPI (D8417, 1 mg/ml stock solution in ultrapure water, Sigma-Aldrich). Specifically, the correlation between the number of nuclei measured in DAPI images and the inhomogeneity measurement was 0.98, $p<0.01$.

Statistical analysis. Data are presented as mean ± standard deviation (mean ± S.D.). Cross correlation was used to estimate the relationship between the number of nuclei in DAPI images and the homogeneity of the bright field images. Continuous baseline variables were compared using the Student's t-test or Mann-Whitney test, accordingly to the variables statistical distribution. Accuracy of linear regression curves was expressed as the coefficient of determination (R^2).

III. RESULTS

In-Vitro Atrial Fibrillation

In Fig. 1A a representative phase map of an *in-vitro* AF episode is shown. In this example, a counterclockwise rotor can be seen in the top-right area of the dish (point 1), whereas several wavebreaks and secondary rotors can be seen in the rest of the dish. After analyzing the DF map, a frequency gradient from the top-right corner to the lower portion of the dish can be observed (Fig. 1B). In Fig. 1C, the time-space plot of the vertical line across the rotor tip in the phase map shows that activity around the main rotor is periodical over time while calcium waves distal from the rotor present an irregular pattern (fragmentation of the propagating wavefronts). The inhomogeneous propagation of wavefronts originating from the stable rotor produced an irregular activation pattern characteristic of AF. Fig. 1D shows the time evolution of calcium transients (CaT) from two camera pixels and their corresponding power spectra. It can be seen that the activation rate of cells distal from the rotor are slower than that of cells around the rotor (i.e. 1.66 Hz vs. 2.84 Hz). The spectral concentration of the frequency components was higher for cells at point 1 than those at point 2, consistent with the decreased activation regularity of cells distal from the rotor.

Relationship between Atrial Tissue Remodeling and Fibrillation Complexity

We observed that the duration of fibrillation significantly modified the complexity of the electrophysiological propagation patterns of HL-1 cells. The number of singularity points per square centimeter at baseline was significantly higher in the late than in the early stage group (i.e. 0.43±0.19 vs. 1.12±0.14 PS/cm^2, $p < 0.01$). In Fig. 2A, normalized CaT and phase map images of a representative cell culture from each group are shown. In the early stage example (left), a single rotor located in the upper-left region of the dish generated relatively regular wavefronts that covered most of the dish (see video 1 in the Online Supplement). However, at the periphery of the dish, small wavebreaks produced a significant number of singularity points. In contrast, several small wavefronts and phase singularities were observed without a clear predominant rotor in late stage cultures (see video 2 in the Online Supplement).

The rotation period of each rotor was measured and the correlation between the fastest rotor and the inverse of the highest dominant frequency was computed for both groups (Fig. 2B). A significant correlation was found between both parameters (i.e. $R^2=0.98$, $p<0.01$), demonstrating that rotors were

responsible for the highest activation rates, which maintained fibrillation in both early and late stage cell cultures.

The increase in the complexity of long term cultures was associated with an electrical remodeling of HL-1 cells as assessed by measuring ionic channel gene expressions (Fig. 2C). RT-PCR analysis showed a significant reduction in the expression of genes CACNA1C, SCN5A and KCND3 which codify for proteins involved in the regulation of L-type calcium channel current (I_{CaL}), voltage activated sodium channel current (I_{Na}) and the transient outward potassium channel current (I_{to}), respectively. In contrast, there was a significant increase in the gene expression of the inward rectifier potassium current, I_{K1}, (i.e. KCNJ2).

The relationship between the structural complexity of HL-1 cell cultures and electrophysiological behavior was evaluated by analyzing the degree of cellular inhomogeneity from bright-field microscopy images. In Fig. 2D, bright-field and immunohistochemistry (i.e. DAPI) microscopy images of two representative examples of HL-1 cell cultures with different degrees of complexity are shown. Longer time cultures were associated with a higher inhomogeneity of bright field images (i.e. 29.56±1.6% of inhomogeneity in the early stage group vs. 33.56±0.6% in the late stage group, $p<0.01$). The number of singularity points per square centimeter showed a direct correlation with the degree of inhomogeneity in the corresponding bright-field microscopy images ($R^2=0.78$, $p<0.01$).

Rotor Dynamics and Fibrillation Complexity

In order to evaluate the electrophysiological mechanisms responsible for increased fibrillation complexity in the late stage group, dominant frequency (DF), mean conduction velocity (CV), rotor curvature and rotor meandering (mean distance traveled for each rotor over time) were measured and compared between groups.

As observed in Fig. 3A, there was no clear correlation between the DF and electrical activity complexity. Furthermore, no significant differences in DFs were found between early and late stage groups (i.e. 3.02 ± 0.56 vs. 2.83 ± 1.43 Hz). According to our results, mechanisms that could explain the increased complexity in the late stage group could be: 1) a reduction in the CV and/or 2) a modification in the rotor dynamics. Although late stage cultures presented a significantly lower CV than the early stage group (i.e. 2.0 ± 0.6 vs. 3.2 ± 1.0 cm/second, $p<0.01$) that could be explained either by a higher cell density or by

the reduction in the expression of I_{Na} (Fig. 2C); the CV had a weak correlation with complexity (i.e. R^2=0.44, Fig. 3B). In contrast, rotor dynamics (i.e. wavefront curvature and rotor meandering) were significantly correlated with electrical complexity (R^2=0.86 and R^2=0.79 respectively, Fig. 3C and 3D).

Analysis of Verapamil-Induced Changes in *In-Vitro* Atrial Fibrillation

To further confirm that fibrillation complexity was mainly governed by rotor dynamics and in order to test the hypothesis that rotors instability could facilitate the termination of AF, fibrillation activity was analyzed 5 minutes following verapamil administration. Verapamil is known to increase the size of the rotor meandering area by means the reduction of the rotor tip excitability (25). Fig. 4 shows phase maps, DF maps and CaTs at baseline and following verapamil administration for a representative example from each group. As shown in the phase maps snapshots, the number of simultaneous rotors and their curvature was significantly reduced following verapamil administration. This reduction in fibrillatory complexity led to a decrease in the activation rate, as shown in the DFs maps and representative CaT signals (Fig. 4).

Fig. 5A shows the effect of verapamil on fibrillation complexity in both cell culture groups. Not only was there a reduction in complexity, but infusion of verapamil resulted in arrhythmia termination after 10 minutes in 5 cell cultures from the early stage group. In addition, for the late stage group, fibrillation complexity following verapamil administration was reduced to values similar to basal conditions of the early stage group (Fig. 5A). This reduction in the complexity was not associated with significant modifications to the CV (Fig. 5B). However, administration of verapamil resulted in a non-uniform decrease of the DF (Fig. 5C); the late stage culture group had higher dominant frequencies after drug infusion as compared to the early stage group. With regards to the rotor dynamics, the average meandering of each rotor significantly increased in both early and late stage groups (Fig. 5D). This increase in the rotor tip movement was associated with a reduction in the rotor curvature in both groups (Fig. 5E). Those modifications in rotor dynamics increased the area needed for each rotor to be self-sustained and could explain the reduction in the complexity.

IV. DISCUSSION

Major findings

The main finding of the present study is that atrial HL-1 cell cultures can reproduce *in-vitro* AF with different degrees of electrophysiological complexity and tissue remodeling resembling processes that occur in AF patients during the transition from paroxysmal to persistent AF. To our knowledge, this is the first study in which the duration of culture has been shown to be correlated with both cell remodeling and the degree of electrophysiological complexity of fibrillation. In addition, our results suggest that rotor dynamics (i.e. meandering and wavefront curvature) play an important role in the formation of complex patterns and could be considered as useful surrogates for the efficacy of novel antiarrhythmic therapies.

Research Models of Chronic Atrial Fibrillation

Atrial tissue remodeling occurs during the transition from paroxysmal to chronic AF, giving rise to more complex fibrillation activity of persistent AF patients (2). Atrial remodeling appears as a consequence of multiple factors, such as ion channel expressions and higher degrees of fibrosis that ultimately results in dilation of the atria and a reduction of atrial contractility (1).

These differences in the electrophysiological mechanisms that govern paroxysmal and chronic AF may explain the observed divergences in the outcome and response to treatment between these two groups of patients (4, 7). A critical obstacle for the elucidation of mechanisms responsible for chronic AF lies in the practical challenges associated with the development of experimental models that reproduce the electrophysiological characteristics of atrial remodeling. Animal models involve subjecting animals to weeks or months of sustained atrial arrhythmias, which implies significant economical, ethical and time burdens (10, 18). Other experimental models include *in-vitro* cell cultures which are typically obtained from neonatal rat hearts. Since neonatal cells do not reproduce the electrophysiological complexity of remodeled tissue, they have been co-cultured with myofibroblasts (31). However, a major drawback is that this model predominantly displays a non-adult ventricular phenotype. In contrast, the HL-1 cell line (8) is the only available cell line that reproduces the features of adult atrial cardiomyocytes (29). In addition, HL-1 cells under fast activation rates present structural and electrophysiological changes such as reduced plasmalemmal levels of L-type Ca^{2+} α1C subunit, myolysis, nuclear condensation and an increase in calpain activity (6), characteristic of remodeled myocytes. Our results are consistent with these experiments and further indicate that HL-1 cells maintained under spontaneously-induced fibrillation

present a reduction in I_{CaL}, I_{Na} and I_{to} ion channels gene expressions and an increase in I_{K1} gene expression. This electrical remodeling is similar to what has been observed in the sheep atrial cardiomyocytes (18) and in patients with long term AF (9).

Mechanisms for an Increased Complexity in Remodeled AF

In the present study we aimed to elucidate the mechanisms that produce an increase in fibrillation complexity in HL-1 cells during long periods of sustained fibrillation. Since the so called funny current (I_f) is present in HL-1 cells, they can develop spontaneous action potentials. Thus, it could be hypothesized that the increase in the complexity of late stage cultures is related to an increased probability of spontaneous cell activation, resulting in more wavebreaks. However, this study demonstrates that functional reentry, and not spontaneous activations or calcium releases, is the underlying mechanism of the sustained fibrillation in both early and late stage HL-1 cell cultures.

The increase in fibrillation complexity in the late stage group was associated with a reduction in tip meandering and an increase of re-entrant wavefront curvature, allowing the formation of more simultaneous rotors. These phenomena are usually associated with shorter action potentials and refractory periods (23), which is consistent with the observed reduction of the I_{CaL} and the increase in I_{K1}. In fact, both computer simulations (14, 22) and experimental studies (26) demonstrated that an unpregulation of I_{K1} is associated with a reduction in rotor tip meandering and a decrease in the area required to maintain the re-entry (22). An additional contribution to fibrillation complexity in our late stage cultures may be an increased cellular heterogeneity in this group. Although the mechanisms of our in-vitro model maybe different, an increased heterogeneity has been found in persistent AF patients mainly due the so-called atrial tissue fibrosis which has shown to promote irregular re-entry formation (19, 31).

Persistent AF is usually characterized by higher DF than paroxysmal AF, both in animals and patients (2, 18). These higher DFs have been associated with a reduction in the time required by a rotor to complete a period due to (1) the reduction of the area of re-entry (i.e. rotor meandering) and (2) an increase of the conduction velocity as a consequence of a higher sodium channel availability consequence of the cell hyperpolarization linked with the I_{K1} upregulation (23). Our results demonstrate that the late stage group presented a reduction in the rotor meandering and an increment of I_{K1} expression which was associated with a higher complexity. However, we did not observe a faster activation rate most likely due to a

reduction of the conduction velocity because of a higher cell density in the late stage group and/or a reduction in the expression of I_{Na} channels.

Interestingly, the administration of verapamil, an L-type calcium channel blocker, resulted in a reduction of fibrillation complexity and a reduction in the DF. This reduction in the DF may seem paradoxical since verapamil shortens the effective refractory period which, in principle, should allow for faster activation rates (21, 24). However this DF reduction can be explained by the modification in the rotor dynamics induced by verapamil; both in the early and late stage groups the blockade of the late calcium current by verapamil increased the area needed for each individual rotor to complete a rotation. The enlargement of the distance that a rotor needs to travel to complete a rotation implies a rotation period lengthening in the absence of CV modifications, and thus a reduction in the DF. This reduction was not uniform in both groups since, after the administration of verapamil, DF of the late stage group was significantly higher than for the early stage group. Concomitantly, a wider rotor tip meandering implies an increment in the probability of collision between rotors. This increased probability of collisions, together with a decrease in the rotor curvature in both groups (Fig. 5E), resulted in a widening of the area required by a rotor to be self-sustained. As a consequence, the number of rotors per area unit was reduced and even terminated in the early stage group. This effect of verapamil on fibrillation complexity is consistent with previous observations in isolated hearts (25) and clinical patients (5) and confirms the important role of calcium homeostasis in mechanisms of AF reentries.

In summary, the results of the present study are in agreement with the contention that rotors play the key role in AF maintenance since the degree of fibrillation complexity depentenimds on reentry curvature and meandering but not necessarily on tissue refractoriness (23). However, the specific mechanisms by which calcium channel blockers increase rotor meandering remain unclear. Further studies are need to clarify the role of calcium currents in reentrant dynamics and more specifically the relation between calcium channels excitability and rotor meandering.

Limitations

The present study was performed by using immortalized murine atrial cells, which are currently the only myocardial cell line with a relatively mature phenotype. HL-1 cell cultures and human atrial tissue present electrophysiological differences evidenced in our results (i.e. a lower DF and CV during fibrillation) and for this reason, extrapolation of these results to human AF should be performed with

care. However, the recent development of human cardiac myocytes derived from pluripotent stem cells (15, 16) may allow the use of *in-vitro* models of human AF in the near future and should serve to extend our study to a more clinically relevant setting. In either case, current limitations in the production of iPS cells and their differentiation into mature cardiomyocytes prevent their extensive application until more efficient production methods are developed.

In the clinical setting, remodeling of atrial tissue takes weeks, months or even years. Here we evaluated differences that occurred in a time interval of a week. These electrophysiological alterations were observable due to the rapid maturation process of HL-1 cells which may be influenced by their continuous proliferation. Hence, specific mechanisms involved in atrial remodeling may differ significantly from those that take place in human chronic AF (6, 27). Nevertheless, in the present study we did not focus on the molecular mechanisms of remodeling but on their impact on electrophysiological properties of fibrillation, and some of these electrophysiological alterations were reproduced in our model.

V. CONCLUSION

HL-1 cells can reproduce AF features such as frequency gradients and mother rotors, giving rise to a hierarchical fibrillatory pattern similar to that described in sheep (17) and human AF (3, 20). In addition, our results demonstrate that the remodeling process of HL-1 cell cultures occurs after several days in culture and resembles that occurring in patients with chronic AF. Modifications in rotor dynamics may underlie the increased complexity of remodeled cell cultures and arise as potential targets for arrhythmia termination. Therefore, this model could be useful for studying the effect of remodeling on fibrillation mechanisms and the development of more effective treatments.

Grants

Supported in part by grants from the Spanish Ministry of Science and Innovation (PLE2009-0152), the Instituto de Salud Carlos III (Ministry of Economy and Competitiveness, Spain: PI13-01882 and PI13-00903) the Red de Investigación Cardiovacular (RIC) from Instituto de Salud Carlos III (Ministry of Economy and Competitiveness, Spain).

Disclosures

Dr. Felipe Atienza served on the advisory board of Medtronic and has received research funding from St. Jude Medical Spain. None of the companies disclosed financed the research described in this manuscript.

REFERENCES

1. **Allessie M, Ausma J, Schotten U.** Electrical, contractile and structural remodeling during atrial fibrillation. *Cardiovasc Res* 54: 230-46, 2002.
2. **Allessie MA, de Groot NM, Houben RP, Schotten U, Boersma E, Smeets JL, Crijns HJ.** Electropathological substrate of long-standing persistent atrial fibrillation in patients with structural heart disease: longitudinal dissociation. *Circ Arrhythm Electrophysiol* 3(6): 606-15 2010.
3. **Atienza F, Almendral J, Jalife J, Zlochiver S, Ploutz-Snyder R, Torrecilla EG, Arenal A, Kalifa J, Fernández-Avilés F, Berenfeld O.** Real-time dominant frequency mapping and ablation of dominant frequency sites in atrial fibrillation with left-to-right frequency gradients predicts long-term maintenance of sinus rhythm. *Heart Rhythm* 6(1): 33-40, 2009.
4. **Atienza F, Almendral J, Ormaetxe JM, Moya A, Martínez-Alday JD, Hernández-Madrid A, Castellanos E, Arribas F, Arias MÁ, Tercedor L, Peinado R, Arcocha MF, Ortiz M, Martínez-Alzamora N, Arenal A, Fernández-Avilés F, Jalife J; RADAR-AF Investigators.** Comparison of Radiofrequency Catheter Ablation of Drivers and Circumferential Pulmonary Vein Isolation in Atrial Fibrillation: A Noninferiority Randomized Multicenter RADAR-AF Trial. *J Am Coll Cardiol* 64(23): 2455-67, 2014.
5. **Bollmann A, Sonne K, Esperer HD, Toepffer I, Klein HU.** Patients with persistent atrial fibrillation taking oral verapamil exhibit a lower atrial frequency on the ECG. *Ann Noninvasive Electrocardiol* 7(2): 92-7, 2002.
6. **Brundel BJ, Kampinga HH, Henning RH.** Calpain inhibition prevents pacing-induced cellular remodeling in a HL-1 myocyte model for atrial fibrillation. *Cardiovasc Res.*1(62): 521-8, 2004.
7. **Calkins H, Kuck KH, Cappato R, Brugada J, Camm AJ, Chen SA, Crijns HJ, Damiano RJ Jr, Davies DW, DiMarco J, Edgerton J, Ellenbogen K, Ezekowitz MD, Haines DE, Haissaguerre M, Hindricks G, Iesaka Y, Jackman W, Jalife J, Jais P, Kalman J, Keane D, Kim YH, Kirchhof P, Klein G, Kottkamp H, Kumagai K, Lindsay BD, Mansour M, Marchlinski FE, McCarthy PM, Mont JL, Morady F, Nademanee K, Nakagawa H, Natale A, Nattel S, Packer DL, Pappone C, Prystowsky E, Raviele A, Reddy V, Ruskin JN, Shemin RJ, Tsao HM, Wilber D; Heart Rhythm Society Task Force on Catheter and**

Surgical Ablation of Atrial Fibrillation. HRS/EHRA/ECAS expert consensus statement on catheter and surgical ablation of atrial fibrillation: Recommendations for patient selection, procedural techniques, patient management and follow-up, definitions, endpoints, and research trial design. *Heart Rhythm* 9: 632-696, 2012.

8. **Claycomb WC, Lanson NA Jr, Stallworth BS, Egeland DB, Delcarpio JB, Bahinski A, Izzo NJ J.** HL-1 cells: a cardiac muscle cell line that contracts and retains phenotypic characteristics of the adult cardiomyocyte. *Proc Natl Acad Sci* 95(6): 2979-84, 1998.
9. **Dobrev D, Ravens U.** Remodeling of cardiomyocyte ion channels in human atrial fibrillation. *Basic Res Cardiol* 98(3): 137-48, 2003.
10. **Filgueiras-Rama D, Price NF, Martins RP, Yamazaki M, Avula UM, Kaur K, Kalifa J, Ennis SR, Hwang E, Devabhaktuni V, Jalife J, Berenfeld O.** Long-term frequency gradients during persistent atrial fibrillation in sheep are associated with stable sources in the left atrium. *Circ Arrhythm Electrophysiol* 5(6): 1160-7, 2012.
11. **Haïssaguerre M, Jaïs P, Shah DC, Takahashi A, Hocini M, Quiniou G, Garrigue S, Le Mouroux A, Le Métayer P, Clémenty J.** Spontaneous initiation of atrial fibrillation by ectopic beats originating in the pulmonary veins. *N Engl J Med* 339(10): 659-66, 1998.
12. **Haralick RM, Shanmugam K, Dinstein I.** Textural Features for Image Classification. *IEEE Trans, on Systems, Man., and Cybernetics* 3: 610-621, 1973.
13. **Jalife J.** Déjà vu in the theories of atrial fibrillation dynamics. *Cardiovasc Res* 89(4): 766-75, 2011.
14. **Koivumäki JT, Seemann G, Maleckar MM, Tavi P.** In silico screening of the key cellular remodeling targets in chronic atrial fibrillation. *PLoS Comput Biol* 10(5): e1003620, 2014.
15. **Lee P, Klos M, Bollensdorff C, Hou L, Ewart P, Kamp TJ, Zhang J, Bizy A, Guerrero-Serna G, Kohl P, Jalife J, Herron TJ.** Simultaneous voltage and calcium mapping of genetically purified human induced pluripotent stem cell-derived cardiac myocyte monolayers. *Circ Res* 110(12): 1556-63, 2012.
16. **Lieu DK, Fu JD, Chiamvimonvat N, Tung KC, McNerney GP, Huser T, Keller G, Kong CW, Li RA.** Mechanism-based facilitated maturation of human pluripotent stem cell-derived cardiomyocytes. *Circ Arrhythm Electrophysiol* 6(1): 191-201, 2013.

17. **Mansour M, Mandapati R, Berenfeld O, Chen J, Samie FH, Jalife J.** Left-to-right gradient of atrial frequencies during acute atrial fibrillation in the isolated sheep heart. *Circulation* 103(21): 2631-6, 2001.

18. **Martins RP, Kaur K, Hwang E, Ramirez RJ, Willis BC, Filgueiras-Rama D, Ennis SR, Takemoto Y, Ponce-Balbuena D, Zarzoso M, O'Connell RP, Musa H, Guerrero-Serna G, Avula UM, Swartz MF, Bhushal S, Deo M, Pandit SV, Berenfeld O, Jalife J.** Dominant frequency increase rate predicts transition from paroxysmal to long-term persistent atrial fibrillation. *Circulation* 129(14): 1472-82, 2014.

19. **McDowell KS, Vadakkumpadan F, Blake R, Blauer J, Plank G, Macleod RS, Trayanova NA.** Mechanistic inquiry into the role of tissue remodeling in fibrotic lesions in human atrial fibrillation. *Biophys J* 104(12): 2764-73, 2013.

20. **Narayan SM, Krummen DE, Shivkumar K, Clopton P, Rappel WJ, Miller JM.** Treatment of atrial fibrillation by the ablation of localized sources: CONFIRM (Conventional Ablation for Atrial Fibrillation With or Without Focal Impulse and Rotor Modulation) trial. *J Am Coll Cardiol* 60(7): 628-36, 2012.

21. **Noguchi K, Masumiya H, Takahashi K, Kaneko K, Higuchi S, Tanaka H, Shigenobu K.** Comparative effects of gallopamil and verapamil on the mechanical and electrophysiological parameters of isolated guinea-pig myocardium. *Can J Physiol Pharmacol* 75(12): 1316-21, 1997.

22. **Pandit SV, Berenfeld O, Anumonwo JM, Zaritski RM, Kneller J, Nattel S, Jalife J.** Ionic determinants of functional reentry in a 2-D model of human atrial cells during simulated chronic atrial fibrillation. *Biophys J* 88(6): 3806-21, 2005.

23. **Pandit SV, Jalife J.** Rotors and the dynamics of cardiac fibrillation. *Circ Res* 112(5): 849-62, 2013.

24. **Riccio ML, Koller ML, Gilmour RF Jr.** Electrical restitution and spatiotemporal organization during ventricular fibrillation. *Circ Res* 84(8): 955-63, 1999.

25. **Samie FH, Mandapati R, Gray RA, Watanabe Y, Zuur C, Beaumont J, Jalife J.** A mechanism of transition from ventricular fibrillation to tachycardia: effect of calcium channel blockade on the dynamics of rotating waves. *Circ Res* 86(6): 684-91, 2000.

26. **Samie FH, Berenfeld O, Anumonwo J, Mironov SF, Udassi S, Beaumont J, Taffet S, Pertsov AM, Jalife J.** Rectification of the background potassium current: a determinant of rotor dynamics in ventricular fibrillation. *Circ Res* 89(12): 1216-23, 2001.
27. **Tsai CT, Chiang FT, Chen WP, Hwang JJ, Tseng CD, Wu CK, Yu CC, Wang YC, Lai LP, Lin JL.** Angiotensin II induces complex fractionated electrogram in a cultured atrial myocyte mono-layer mediated by calcium and sodium-calcium exchanger. *Cell Calcium* 49(1): 1-11, 2011.
28. **Tsai CT, Chiang FT, Tseng CD, Yu CC, Wang YC, Lai LP, Hwang JJ, Lin JL.** Mechanical stretch of atrial myocyte monolayer decreases sarcoplasmic reticulum calcium adenosine triphosphatase expression and increases susceptibility to repolarization alternans. *J Am Coll Cardiol* 58(20): 2106-15, 2011.
29. **White SM, Constantin PE, Claycomb WC.** Cardiac physiology at the cellular level: use of cultured HL-1 cardiomyocytes for studies of cardiac muscle cell structure and function. *Am J Physiol Heart Circ Physiol* 286(3): H823-9, 2004.
30. **Wijffels MC, Kirchhof CJ, Dorland R, Allessie MA.** Atrial fibrillation begets atrial fibrillation. A study in awake chronically instrumented goats. *Circulation* 92(7): 1954-68, 1995.
31. **Zlochiver S, Muñoz V, Vikstrom KL, Taffet SM, Berenfeld O, Jalife J.** Electrotonic myofibroblast-to-myocyte coupling increases propensity to reentrant arrhythmias in two-dimensional cardiac monolayers. *Biophys J* 95(9): 4469-80, 2008.

FIGURE LENGEDS

Fig. 1. Illustrative example of in-vitro early stage atrial fibrillation. A, Phase map of calcium transients showing a fast stable rotor at the top-right area of the dish. B, Dominant frequency map demonstrating a frequency gradient from the top-right to the lower region of the dish. C, Time-space plot of activity across the line defined by points 1 and 2, as shown in panel A. D, Time series of calcium transient optical signals (left) and their corresponding power spectrum (right), from points 1 and 2

Fig. 2. Comparison between early and late stage cell cultures. A, CaT and phase maps of representative cell culture monolayers from each group. B, Correlation between the shortest rotation period and dominant cycle length (1/DF). C, Expression of genes CACNA1C, SNC5A, KCND3 and KCNJ2 in early and late stage groups. These genes codify for proteins which are molecular components of ion channels associated with I_{CaL}, I_{Na}, I_{To} and I_{K1} currents, respectively. D, Representative examples of bright-field and DAPI images for the early and late stage cell cultures. *p< 0.05, **p< 0.01.

Fig. 3. Correlation between the electrophysiological complexity, measured as the number of phase singularities per square centimeter, and (A) highest dominant frequency, (B) mean conduction velocity, (C) rotor curvature and (D) rotor meandering.

Fig. 4. Effects of verapamil on activation maps and the frequency domain. Snapshots of phase maps (top) and dominant frequency maps (bottom) during basal conditions (left) and after administration of verapamil (right) in an illustrative case for (A) early and (B) late stage groups. Time series of calcium transient optical signals (left) and the corresponding power spectrum (right) of the starred region during basal conditions (top) and after the administration of verapamil (bottom) for the (C) early stage and (D) late stage groups.

Fig. 5. Quantification of verapamil effects on the electrophysiological characteristics of both early and late stage culture groups. A, Complexity measured as the number of simultaneous phase singularities per square centimeter. B, Conduction velocity. C, Dominant frequency. D, Rotor meandering (mean distance traveled for each rotor over time). E, Mean curvature of rotors. *p< 0.05, **p< 0.01

TABLE 1

Table 1. Primers used for reverse transcription polymerase chain reaction (RT-PCR).

Gene	Protein	Forward Primer (5'->3')	Reverse Primer (5'->3')
CACNA1C	Cav 1.2	CCTCGAAGCTGGGAGAACAG	TGTGTGGGAGTCAATGGAGC
SCN5A	Nav1.5	CACCTTCACCGCCATCTACA	AAGGTGCGTAAGGCTGAGAC
KCND3	Kv 4.3	TGCCTAAGACAATCGCAGGG	TGTGCAGGTAGGCATTGGAG
KCNJ2	Kir 2.1	GACGCCTTCATCATTGGTGC	CCGGACATGAGCTTCCACAA
36B4		GCGACCTGGAAGTCCAACTA	ATCTGCTGCATCTGCTTGG
CYCLOPHYLIN		ACAGGTCCTGGCATCTTGTC	CATGGCTTCCACAATGTTCA

FIG. 1

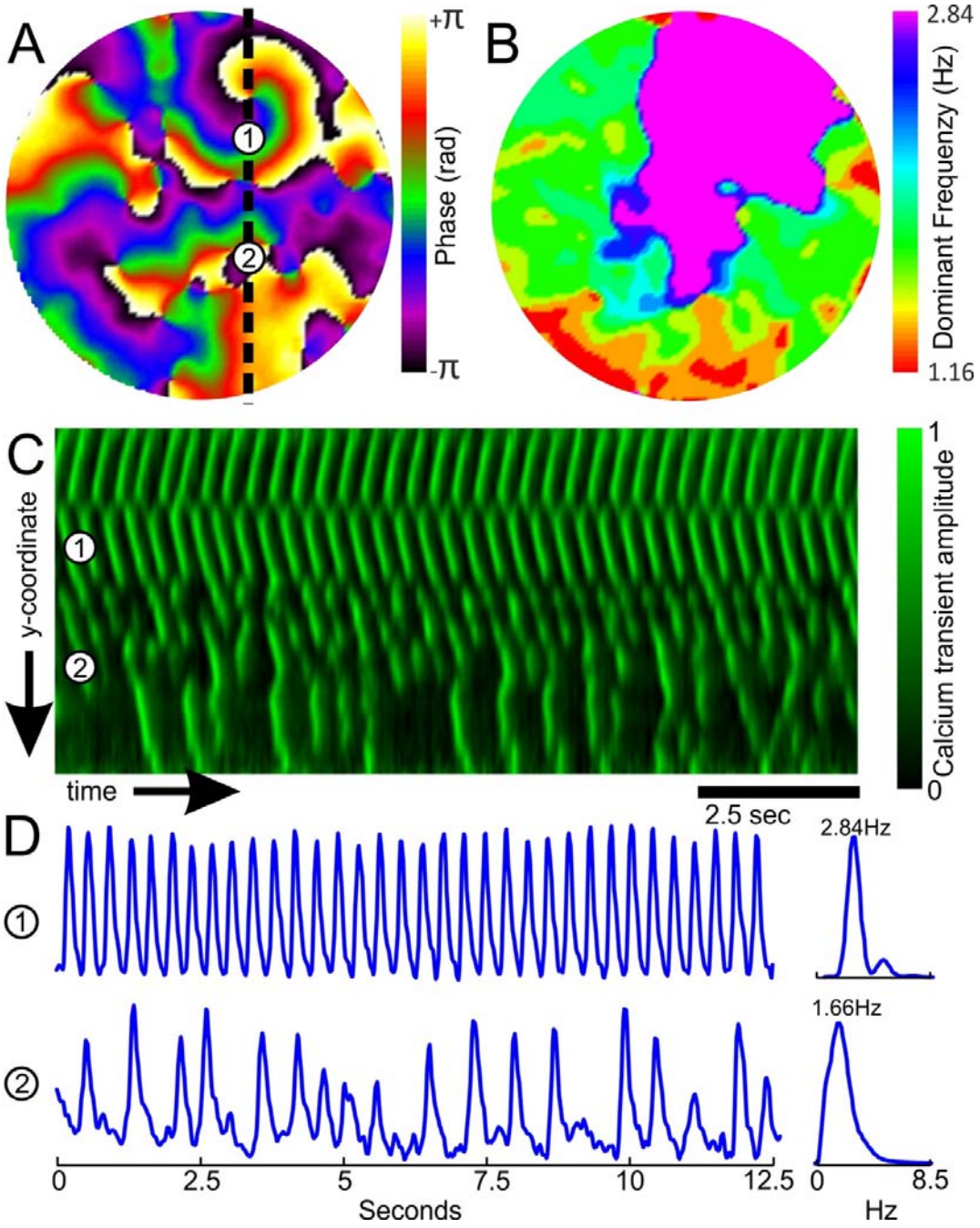
A
+π
Phase (rad)
-π
B
2.84
Dominant Frequenzy (Hz)
1.16
C
y-coordinate
1
2
time
2.5 sec
1
Calcium transient amplitude
0
D
2.84Hz
1.66Hz
0
2.5
5
7.5
10
12.5
Seconds
0
8.5
Hz

.

494 **FIG. 2**

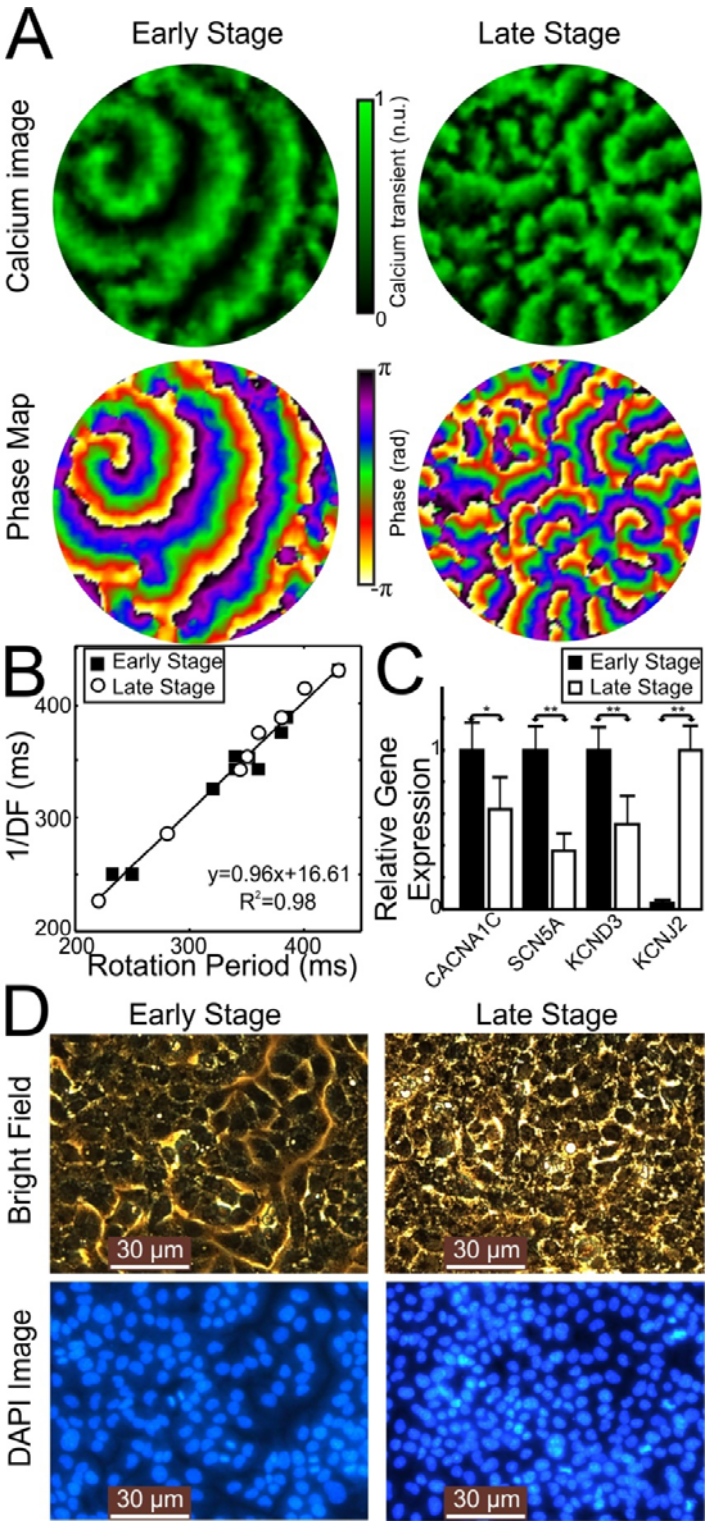

495

496

497 **FIG. 3**

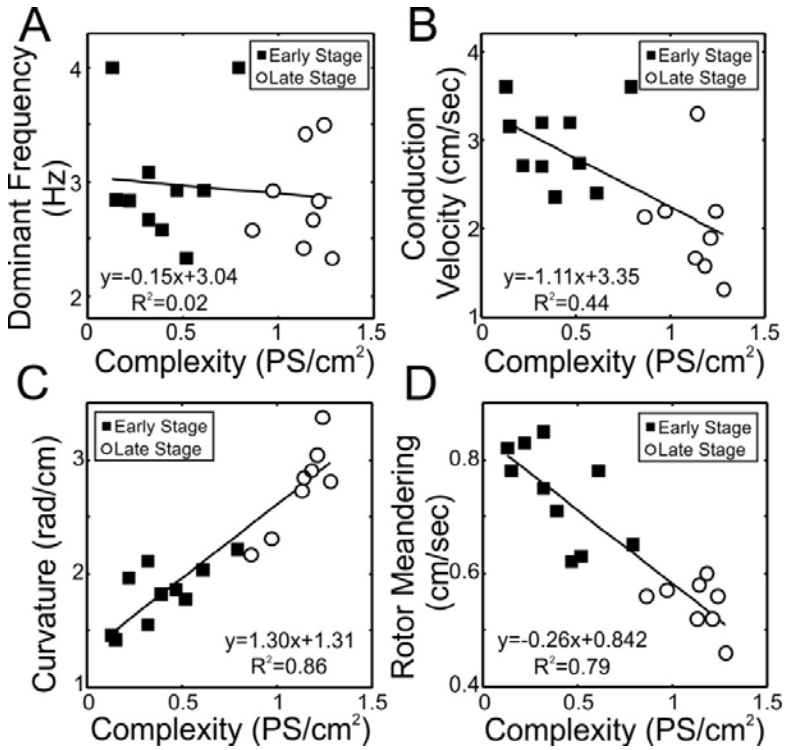

498

499

FIG. 4

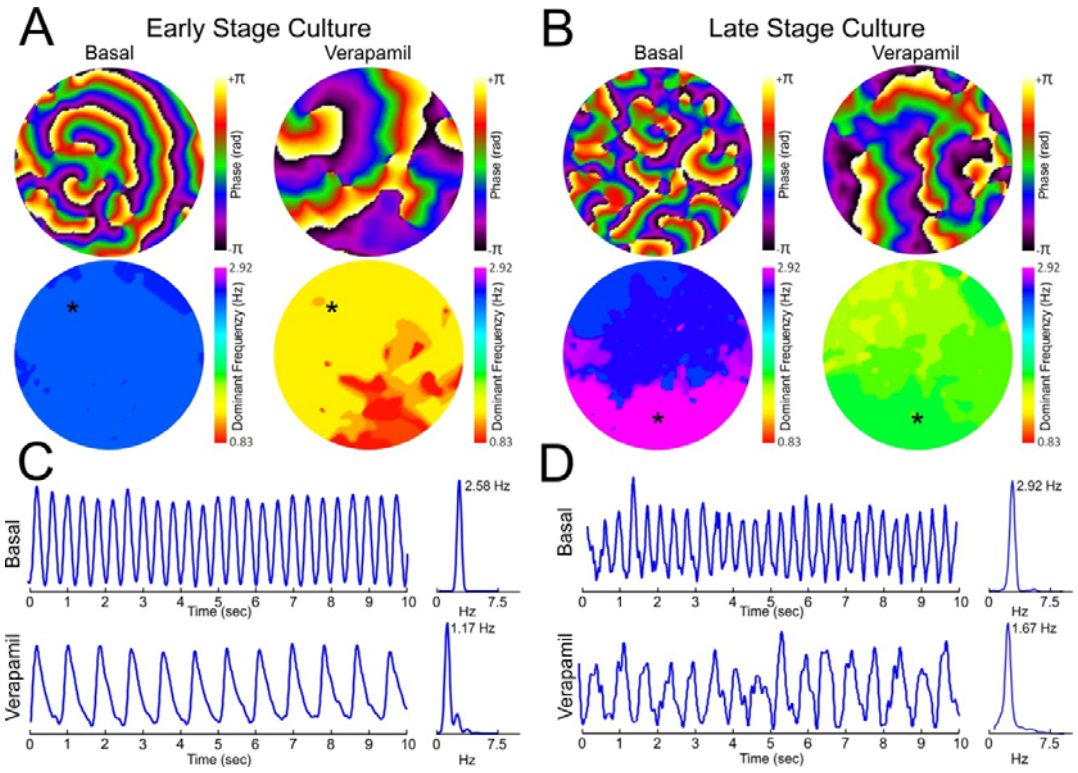
A
Early Stage Culture
Basal
Verapamil
B
Late Stage Culture
Basal
Verapamil
+π
-π
Phase (rad)
2.92
0.83
Dominant Frequency (Hz)
C
D
Basal
Verapamil
Time (sec)
2.58 Hz
1.17 Hz
2.92 Hz
1.67 Hz
Hz

504 **FIG. 5**

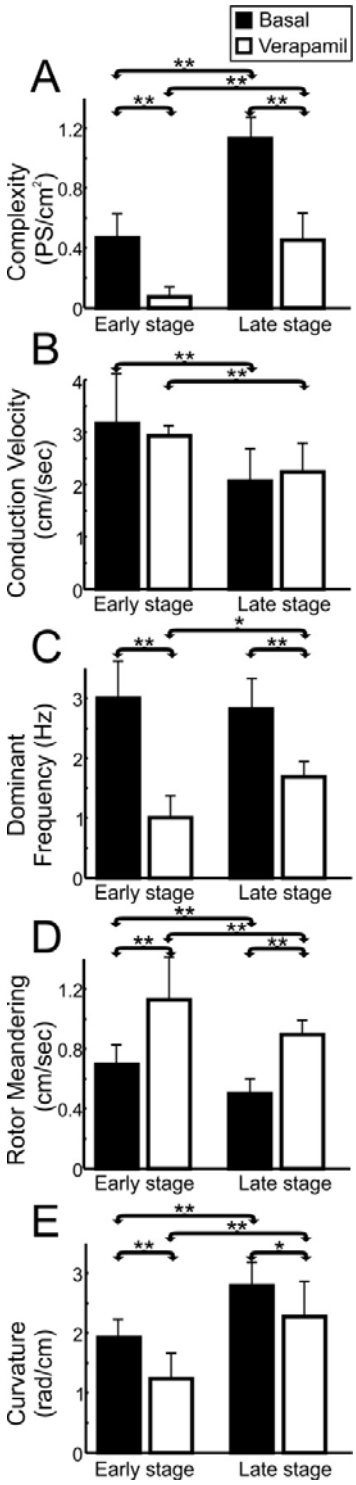

505

506

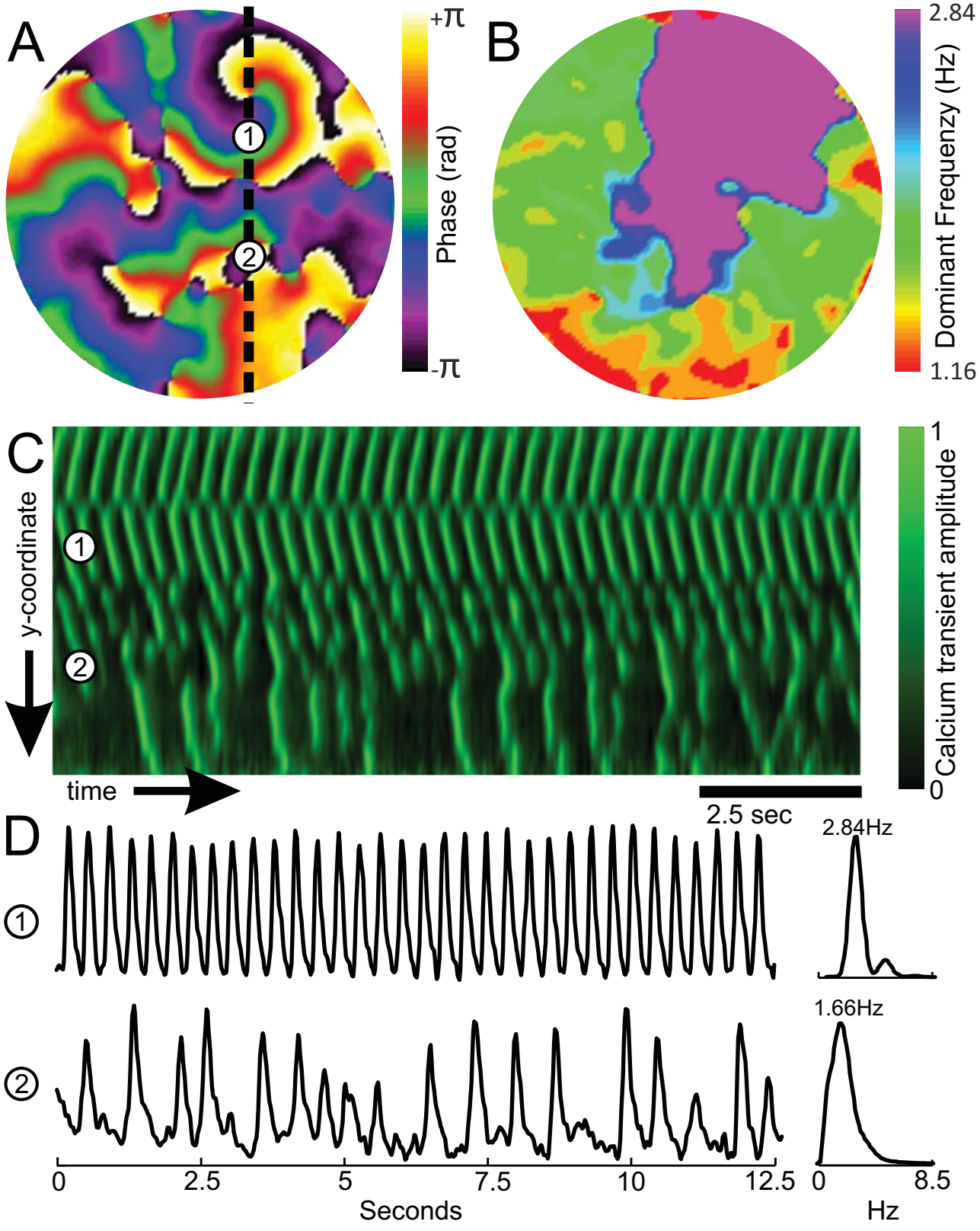
A
+π
Phase (rad)
-π
1
2
B
2.84
Dominant Frequency (Hz)
1.16
C
y-coordinate
1
2
time
2.5 sec
1
Calcium transient amplitude
0
D
1
2
2.84Hz
1.66Hz
0
2.5
5
7.5
10
12.5
Seconds
0
8.5
Hz

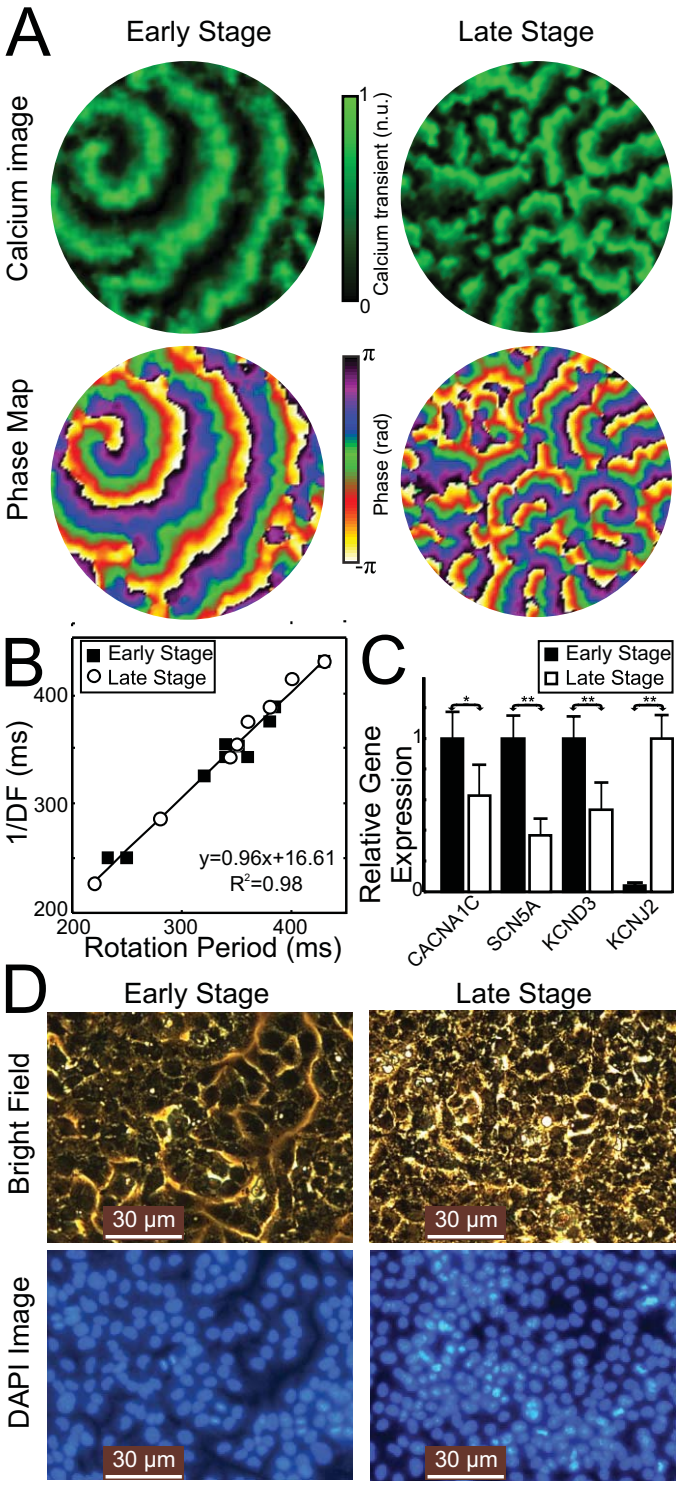
A
Early Stage
Late Stage
Calcium image
Calcium transient (n.u.)
1
0
Phase Map
Phase (rad)
π
-π
B
Early Stage
Late Stage
1/DF (ms)
400
300
200
200
300
400
Rotation Period (ms)
y=0.96x+16.61
R²=0.98
C
Early Stage
Late Stage
Relative Gene Expression
1
0
*
**
**
**
CACNA1C
SCN5A
KCND3
KCNJ2
D
Early Stage
Late Stage
Bright Field
30 μm
30 μm
DAPI Image
30 μm
30 μm

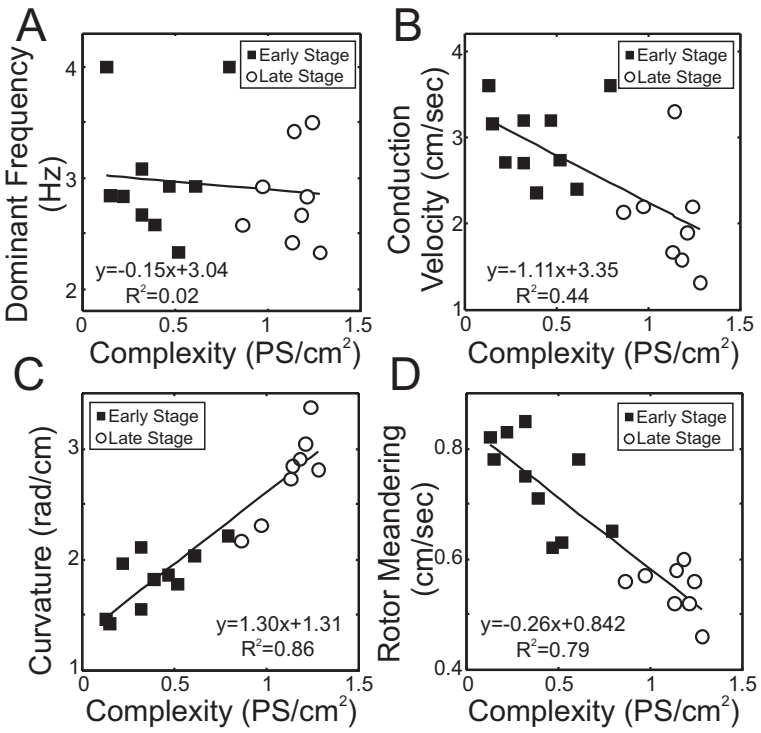
A
Dominant Frequency (Hz)
Early Stage
Late Stage
y=-0.15x+3.04
R²=0.02
Complexity (PS/cm²)
B
Conduction Velocity (cm/sec)
Early Stage
Late Stage
y=-1.11x+3.35
R²=0.44
Complexity (PS/cm²)
C
Curvature (rad/cm)
Early Stage
Late Stage
y=1.30x+1.31
R²=0.86
Complexity (PS/cm²)
D
Rotor Meandering (cm/sec)
Early Stage
Late Stage
y=-0.26x+0.842
R²=0.79
Complexity (PS/cm²)

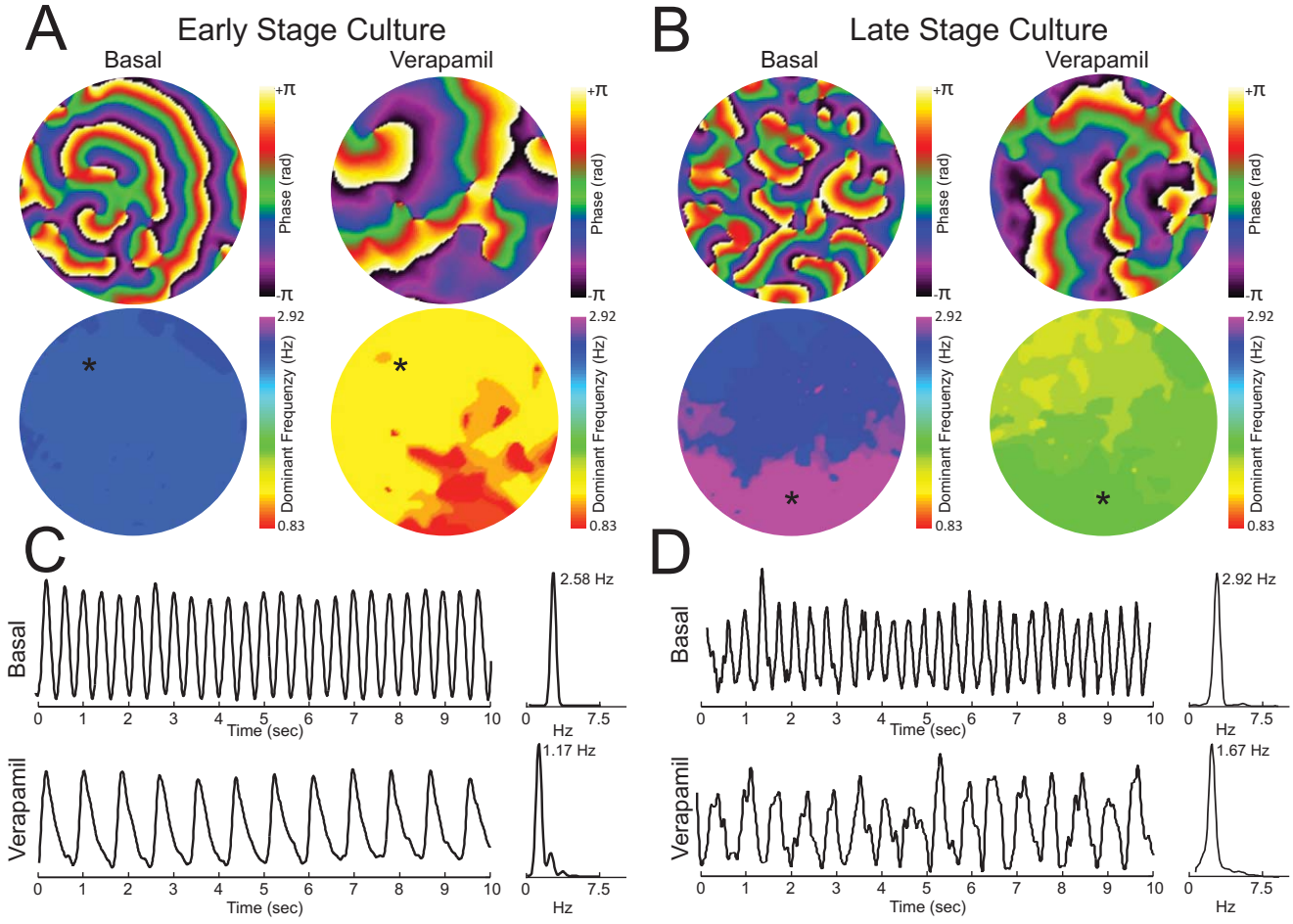
A
Early Stage Culture
Basal
Verapamil
+π
-π
Phase (rad)
2.92
0.83
Dominant Frequenzy (Hz)
B
Late Stage Culture
C
D
Basal
Verapamil
Time (sec)
2.58 Hz
1.17 Hz
2.92 Hz
1.67 Hz
Hz

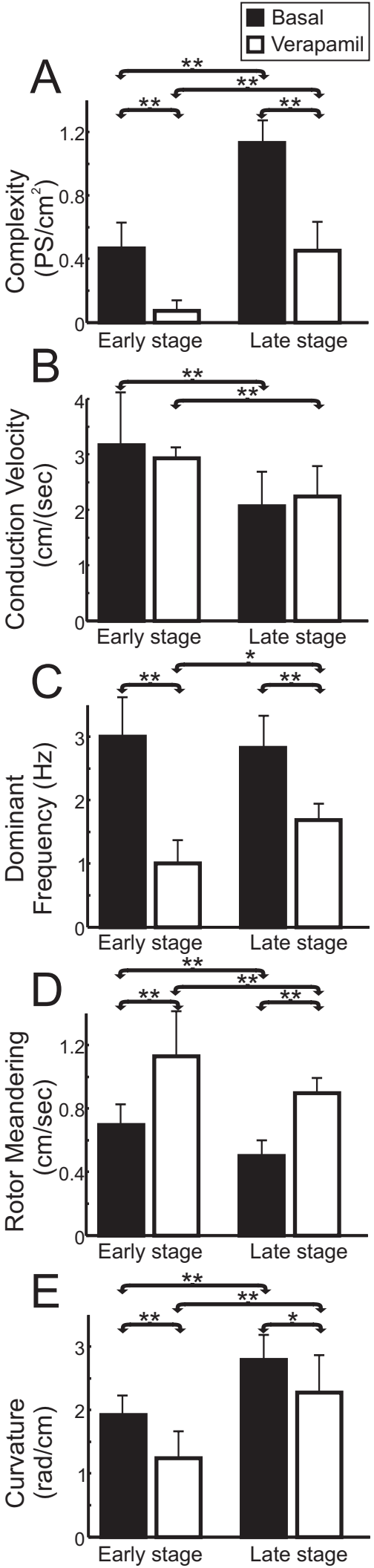
Basal
Verapamil
A
Complexity (PS/cm^2)
1.2
0.8
0.4
0
**
**
**
**
Early stage
Late stage
B
Conduction Velocity (cm/(sec)
4
3
2
1
0
**
**
Early stage
Late stage
C
Dominant Frequency (Hz)
3
2
1
0
**
*
**
Early stage
Late stage
D
Rotor Meandering (cm/sec)
1.2
0.8
0.4
0
**
**
**
**
Early stage
Late stage
E
Curvature (rad/cm)
3
2
1
0
**
**
*
**
Early stage
Late stage